

## Positive quantum magnetoresistance in tilted magnetic field

William Mayer, Areg Ghazaryan, Pouyan Ghaemi, and Sergey Vitkalov\*  
*Physics Department, City College of the City University of New York, New York 10031, USA*

A. A. Bykov

*A. V. Rzhanov Institute of Semiconductor Physics, Novosibirsk 630090, Russia  
 and Physics Department, Novosibirsk State University, Novosibirsk 630090, Russia*

(Received 25 August 2016; revised manuscript received 7 October 2016; published 23 November 2016)

Transport properties of highly mobile 2D electrons are studied in symmetric GaAs quantum wells placed in tilted magnetic fields. Quantum positive magnetoresistance (QPMR) is observed in magnetic fields perpendicular to the 2D layer. Application of in-plane magnetic field produces a dramatic decrease of the QPMR. This decrease correlates strongly with the reduction of the amplitude of Shubnikov–de Haas resistance oscillations due to modification of the electron spectrum via enhanced Zeeman splitting. Surprisingly no quantization of the spectrum is detected when the Zeeman energy exceeds half of the cyclotron energy suggesting an abrupt transformation of the electron dynamics. Observed angular evolution of QPMR implies strong mixing between spin subbands. Theoretical estimations indicate that in the presence of spin-orbital interaction the elastic impurity scattering provides significant contribution to the spin mixing in GaAs quantum wells at high filling factors.

DOI: [10.1103/PhysRevB.94.195312](https://doi.org/10.1103/PhysRevB.94.195312)

### I. INTRODUCTION

The orbital quantization of electron motion in magnetic fields generates a great variety of fascinating transport phenomena observed in condensed materials. Shubnikov–de Haas (SdH) resistance oscillations [1] and the quantum Hall effect (QHE) [2] are famous examples. Spin degrees of freedom enrich the electron response [3,4]. In two-dimensional (2D) electron systems the orbital quantization is due to the component of the magnetic field,  $B_{\perp}$ , which is perpendicular to the 2D layer [5] whereas the spin degrees of freedom are affected mostly by the total magnetic field  $B$  [6]. An increase of the in-plane magnetic field produces, thus, an enhancement of the spin splitting (Zeeman effect),  $\Delta_Z = \mu g B$ , with respect to the cyclotron energy,  $\Delta_C = \hbar\omega_c$ . Here  $\mu$  is the Bohr magneton,  $g$  is the  $g$  factor,  $\omega_c = eB_{\perp}/m = eB \cos(\alpha)/m$  is the cyclotron frequency,  $m$  is the electron effective mass, and  $\alpha$  is the angle between magnetic field  $\vec{B}$  and the normal  $\vec{n}$  to the 2D layer. At a critical angle  $\alpha_c$  corresponding to the condition

$$\Delta_Z = \frac{\Delta_C}{2} \Leftrightarrow \cos(\alpha_c) = \frac{gm}{m_0}, \quad (1)$$

where parameter  $m_0$  is mass of the free electron, quantum levels are equally separated by  $\hbar\omega_c/2$  and the amplitude of the fundamental harmonic of SdH oscillations,  $A_{SdH}$ , is zero. This property is the basis of a powerful transport method (coincidence method) for the study of the spin degrees of freedom of 2D electrons [3,6].

In GaAs quantum wells the critical angle  $\alpha_c$  is large,  $\alpha_c \approx 85^{\circ} - 87^{\circ}$ , due to a small effective electron mass [7–10]. At low temperatures,  $kT \ll \Delta_c$ , the coincidence method yields the  $g$  factor, which is considerably larger than the one obtained from electron spin resonance [11,12]. An even stronger spin gap is found in measurements of the activation temperature dependence of the magnetoresistance [7,8]. The enhancement

of the spin splitting is attributed to effects of electron-electron interaction of 2D electrons [3]. At low temperatures and high filling factors the spin splitting is found to be proportional to  $B_{\perp}$  [8,13,14], which agrees with theoretical evaluations of the contribution of the  $e-e$  interaction to the spin gap, when only one quantum level is partially filled [15].

The enhancement of the spin splitting is found above a sample-dependent critical magnetic field  $B_c$  [8,9,16]. This effect has been attributed to the suppression of the contributions of the  $e-e$  interaction to the spin splitting by a static disorder [17]. With an increase of the temperature from the mK range to a few kelvins the  $g$ -factor enhancement ( $B_c$ ) is found to be decreasing (increasing) considerably, which is attributed to a reduction of the contribution of the  $e-e$  interaction to the spin splitting due to thermal fluctuations [8].

At high temperatures,  $kT \gg \Delta_C, \Delta_Z$  there are many partially populated Landau levels participating in transport and one may expect a quantitatively different value of the  $e-e$  enhanced spin splitting in comparison with the one at  $kT \ll \Delta_C, \Delta_Z$ . We note that the spin splitting has not been investigated experimentally in the quantized spectrum at high temperatures since the coincidence method relies on SdH oscillations, which are absent (exponentially suppressed) in the high-temperature regime [1]. Recent developments [18] open a possibility to study spin effects in electron systems with a quantized spectrum at high temperatures:  $kT \gg \Delta_C, \Delta_Z$ .

This paper presents an experimental investigation of the quantum positive magnetoresistance (QPMR) at high temperatures  $kT \gg \Delta_C, \Delta_Z$  and SdH resistance oscillations in GaAs symmetric quantum wells placed in tilted quantizing magnetic fields. The experiments indicate that angular variations of the QPMR and the SdH amplitude strongly correlate yielding essentially the same  $g$  factor:  $g \approx 0.97 \pm 0.08$ . This  $g$ -factor value is close to the one obtained in experiments done at much lower temperatures [7–10].

At a fixed  $B_{\perp} > 0.3$  T the angular evolution of QPMR demonstrates a resistance maximum at  $\alpha \approx 62^{\circ}$ , revealing an unexpected decrease of the spin splitting with the in-plane

\*Corresponding author: [svitkalov@ccny.cuny.edu](mailto:svitkalov@ccny.cuny.edu)

magnetic fields while the overall angular evolution of QPMR demonstrates  $B/B_{\perp}$  scaling at  $\Delta_Z/\Delta_C < 1/2$  ( $\alpha < 86^\circ$ ). At  $\alpha > 86^\circ$  the QPMR does not return as expected indicating an absence of the quantized electron spectrum in the high-temperature and large-parallel-field regime. A complementary study of quantal heating [19–21] at different angles confirms this observation.

In contrast to SdH oscillations the angular evolution of QPMR implies a significant mixing between spin-up and spin-down subbands due to quadratic dependence of the conductivity on DOS [see Eq. (4)]. When the spin and momentum of the electrons are independent, the nonmagnetic impurities cannot mix the electronic states with opposite spins. On the other hand in the presence of spin-orbit coupling, the spin and momentum of electrons are not independent. In contrast to the Zeeman splitting the spin-orbit interaction depends on the energy (velocity) of electrons and does not decrease at small magnetic fields [22,23]. As we show below, even at a small spin-orbit coupling local nonmagnetic impurities may lead to a scattering between different subsets of quantum levels leading to the spin mixing at high filling factors.

## II. EXPERIMENTAL SETUP

Studied GaAs quantum wells were grown by molecular beam epitaxy on a semi-insulating (001) GaAs substrate. The material was fabricated from a selectively doped GaAs single quantum well of width  $d = 13$  nm sandwiched between AlAs/GaAs superlattice barriers. The studied samples were etched in the shape of a Hall bar. The width and the length of the measured part of the samples are  $W = 50 \mu\text{m}$  and  $L = 250 \mu\text{m}$ . AuGe eutectic was used to provide electric contacts to the 2D electron gas. Two samples were studied at temperature 4.2 K in magnetic fields up to 9 T applied *in situ* at different angles  $\alpha$  relative to the normal to 2D layers and perpendicular to the applied current. The angle  $\alpha$  has been evaluated using Hall voltage  $V_H = B_{\perp}/(en_T)$ , which is proportional to the perpendicular component,  $B_{\perp} = B \cos(\alpha)$ , of the total magnetic field  $B$ . The total electron density of samples,  $n_T \approx 8.6 \times 10^{11} \text{ cm}^{-2}$ , was evaluated from the Hall measurements taken at  $\alpha = 0^\circ$  in classically strong magnetic fields [24]. An average electron mobility  $\mu \approx 1.6 \times 10^6 \text{ cm}^2/\text{Vs}$  was obtained from  $n_T$  and the zero-field resistivity. Sample resistance was measured using the four-point probe method. We applied a 133 Hz *ac* excitation  $I_{ac} = 1 \mu\text{A}$  through the current contacts and measured the longitudinal (in the direction of the electric current,  $x$  direction) and Hall *ac* (along  $y$  direction) voltages ( $V_{xx}^{ac}$  and  $V_H^{ac}$ ) using two lock-in amplifiers with 10 M $\Omega$  input impedances. The measurements were done in the linear regime in which the voltages are proportional to the applied current.

## III. RESULTS AND DISCUSSION

Figure 1 presents the dissipative resistivity,  $\rho_{xx}(B_{\perp})$ , at different angles  $\alpha$  between the magnetic field,  $B$ , and the normal to the 2D layer,  $\vec{n}$ . In perpendicular magnetic fields below 0.11 T the resistance is nearly (within  $\sim 0.6$ ) independent of  $B_{\perp}$ . This is the regime of classical (Drude) magnetoresistance, which is expected to be independent of  $B_{\perp}$  [24].

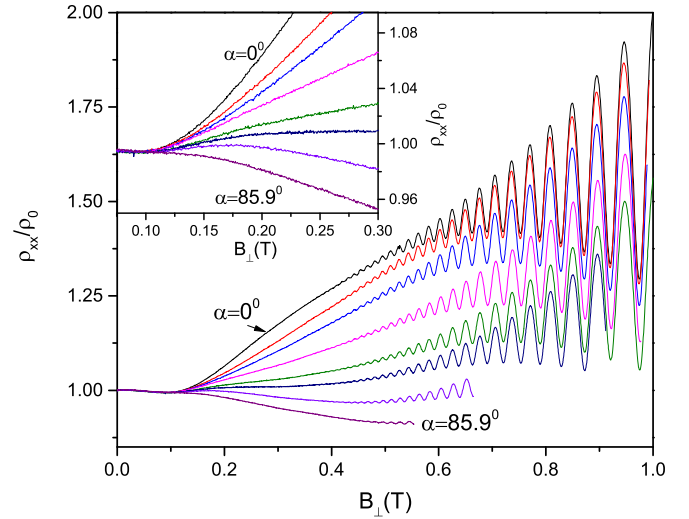


FIG. 1. Dependence of the longitudinal resistance  $\rho_{xx}$  on the magnetic field perpendicular to the 2D sample obtained at different angles  $\alpha$  between the total magnetic field  $B$  and the normal to the 2D layer. From the top curve to the bottom one angles are 0, 76.2, 78.6, 81.2, 82.6, 83.13, 84, and 85.9 degrees. The inset enlarges the area at small magnetic fields indicating that the dependencies at different angles diverge from approximately the same magnetic field  $B^* \approx 0.11$  T corresponding to the beginning of Landau quantization of the electron spectrum at  $\alpha = 0^\circ$ .

At  $\alpha = 0^\circ$  and  $B_{\perp} > 0.11$  T the magnetoresistance demonstrates a steep (exponential in  $1/B_{\perp}$ ) monotonic increase combined with SdH oscillations in  $B_{\perp} > 0.45$  T. This increase is attributed [18] to the quantum positive magnetoresistance (QPMR) due to Landau quantization [25]. At angles  $\alpha < 65^\circ$  and  $B_{\perp} > 0.33$  T the magnetoresistance exhibits an additional few percent increase with the angle (not shown). At  $\alpha > 65^\circ$  the QPMR decreases significantly with the angle. Figure 1 demonstrates this decrease for angles between 76.2 and 85.9 degrees. The inset to the figure shows that the angular variation of QPMR is approximately uniform with  $B_{\perp}$  and starts at the same perpendicular magnetic field  $B^* \approx 0.11$  T, which separates the classical and quantum regimes of electron transport [18,25]. The later indicates that the Landau level width (or the quantum scattering time  $\tau_q$ ) is nearly independent of angle  $\alpha$ . This is confirmed by more detailed comparison [see Fig. 3(d)]. At angles  $\alpha > 86^\circ$  the QPMR demonstrates a weak recovery (not shown), which is discussed later.

At  $B_{\perp} > 0.45$  T, Fig. 1 shows SdH oscillations. In contrast to QPMR the angular evolution of SdH oscillations has been intensively studied [7,8,10]. The presented experiments show strong correlation between angular evolutions of SdH oscillations and QPMR. Before the detailed discussion and comparison of the dependencies, we present a model, which captures the strong angular correlations of these two phenomena.

### A. Model of SdH oscillations and quantum positive magnetoresistance

A microscopic description of both SdH oscillations and QPMR in perpendicular magnetic fields (at  $\alpha = 0^\circ$ ) is presented in Ref. [25] neglecting any spin-related effects, in

particular the Zeeman term. As indicated in the Introduction the account of the Zeeman splitting for SdH oscillations is a developed procedure [3,6,8]. In contrast the spin-related effects in the QPMR have not been studied yet.

Below we present a model that utilizes the similarity of QPMR and magneto-intersubband (MISO) resistance oscillations [26–30]. The model considers two subbands with the energy spectrum evolving in accordance with Landau quantization and split predominantly by the Zeeman effect [6]. A scattering-assisted mixing between different subbands is postulated to provide the observed correlation between the angular evolutions of SdH oscillations and QPMR. Within the presented model the absence of the scattering between subbands would lead to the absence of an angular evolution of the QPMR associated with the Zeeman effect in contrast to the angular dependence of SdH oscillations. The origin of the mixing requires further investigations. A mixing between different spin subbands has been reported in Si-MOSFETs [31]. The experiments show a sizable contribution of the product of the spin-up and spin-down density of states to SdH resistance oscillations. Furthermore investigations of the resistivity tensor in tilted magnetic fields have revealed an independence of the Hall coefficient on the spin subband populations while the electron mobility in each spin subband was substantially affected by the in-plane magnetic field [32]. This behavior has been interpreted by a mixing between spin subbands due to an electron-electron interaction [33]. We note also that in the presence of a spin-orbit coupling, different subbands could be mixed by a local impurity scattering. An investigation of this possibility is presented in Sec. III D.

In the simplest case of small quantizing magnetic fields  $\omega_c \tau_q < 1$  the main contribution to both SdH oscillation and QPMR comes from the fundamental harmonic of quantum oscillations of the density of states (DOS) corresponding to spin-up and spin-down subbands. The total DOS,  $\nu(\epsilon)$ , reads [3]

$$\begin{aligned} \nu(\epsilon) &= \nu_0 \left[ 1 - \delta \cos \left( \frac{2\pi(\epsilon - \Delta_Z/2)}{\hbar\omega_c} \right) \right. \\ &\quad \left. - \delta \cos \left( \frac{2\pi(\epsilon + \Delta_Z/2)}{\hbar\omega_c} \right) \right] \\ &= \nu_0 \left[ 1 - 2\delta \cos \left( \frac{2\pi\epsilon}{\hbar\omega_c} \right) \cos \left( \frac{\pi\Delta_Z}{\hbar\omega_c} \right) \right], \end{aligned} \quad (2)$$

where  $\delta = \exp(-\pi/\omega_c \tau_q)$  is the Dingle factor,  $\nu_0$  is the total DOS at zero magnetic field, and  $\tau_q$  is the quantum scattering time, which is considered to be the same in both spin subbands.

The 2D conductivity  $\sigma$  is obtained from the following relation:

$$\sigma(B) = \int d\epsilon \sigma(\epsilon) \left( -\frac{\partial f}{\partial \epsilon} \right) = \langle \sigma(\epsilon) \rangle. \quad (3)$$

The integral is an average of the conductivity  $\sigma(\epsilon)$  taken essentially for energies  $\epsilon$  inside the temperature interval  $kT$  near Fermi energy, where  $f(\epsilon)$  is the electron distribution function at the temperature  $T$  [3]. The brackets represent this integral below.

The following expression approximates the conductivity  $\sigma(\epsilon)$  at small quantizing magnetic fields:

$$\sigma(\epsilon, B_\perp, \Delta_Z) = \sigma_D(B_\perp) \tilde{\nu}(\epsilon, B_\perp, \Delta_Z)^2, \quad (4)$$

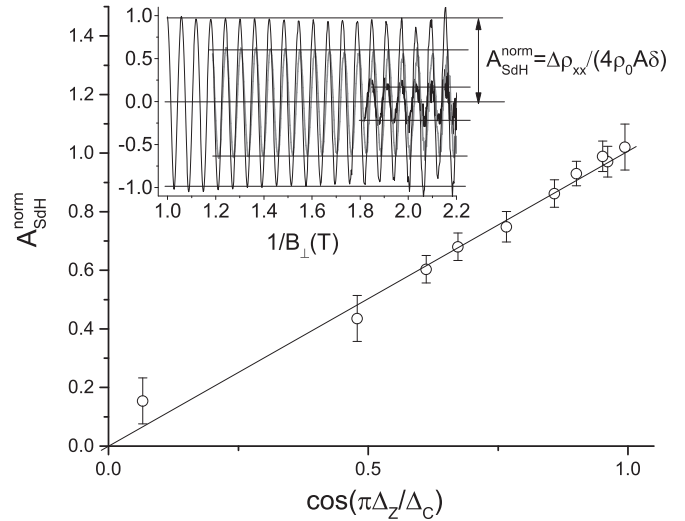


FIG. 2. Dependence of normalized amplitude of SdH oscillations,  $A_{SdH}^{norm} = A_{SdH}/4\delta A(T)$ , on  $\cos(\pi\Delta_Z/\Delta_C)$  with  $g = 0.97$ . The dependence corresponds to Eq. (5) relating the angular evolution of SdH amplitude to the angular variation of the ratio between Zeeman and cyclotron energies:  $\Delta_Z/\Delta_C = mg/(2m_0 \cos \alpha)$ . The inset presents normalized SdH resistance oscillations in reciprocal magnetic fields at angles  $\alpha$ : 67.6, 83.3, and 85.9 degrees.

where  $\sigma_D(B_\perp)$  is Drude conductivity in magnetic field  $B_\perp$  [24] and  $\tilde{\nu}(\epsilon) = \nu(\epsilon)/\nu_0$  is the normalized total density of states. The main assumption of this model is utilized in Eq. (4). Namely the impurity scattering between the spin-up and spin-down subbands is considered to be comparable with the impurity scattering within a spin subband, when the energies of the spin sectors are the same. In other words a spin-up (spin-down) electron has equal probability to scatter into a spin-up or spin-down quantum state.

The proportionality of the conductivity  $\sigma(\epsilon)$  to the square of the normalized density of states is due to two factors. One factor takes into account the number of available conducting states (parallel channels) at energy  $\epsilon$ , which is proportional to the density of states. The second factor takes into account that the dissipative conductivity in crossed electric and magnetic fields is proportional to the electron scattering rate [24]. At low temperatures the scattering is dominated by the elastic impurities making the rate proportional to the density of final states at the same energy  $\epsilon$  [24,34]. The quadratic dependence of the conductivity on the density of state results in the factor 4 in Eq. (5), which is found to be in good quantitative agreement with the amplitude of SdH oscillations shown in Fig. 2. Furthermore the quadratic dependence on the density of states yields both QPMR and its strong correlation with SdH oscillations observed in presented experiments.

Equation (4) is similar to Eq. (5) of Ref. [35], which was used for the conductivity in the perpendicular magnetic fields neglecting both the Zeeman splitting and spin-orbital effects. In this case the energy spectrum of spin-up and spin-down electrons is the same and the normalized DOS for each spin subband coincides with the normalized total DOS,  $\tilde{\nu}(\epsilon)$ . For two independent spin subbands the total conductivity is the sum of two terms:  $\sigma_{ind} = \sigma^+ + \sigma^-$ , where  $\sigma^\pm = (\sigma_D/2)\tilde{\nu}(\epsilon)^2$ . The factor 1/2 takes into account that the electron density in

each subband is half the total density. Thus at  $\Delta_Z = 0$  the total conductivity of two subbands does not depend on the intersubband scattering:  $\sigma_{\text{ind}} = \sigma(\Delta_Z = 0)$ . At finite  $\Delta_Z$  the intersubband scattering affects the conductivity.

A substitution of Eq. (4) and Eq. (2) into Eq. (3) yields two additional terms to the Drude conductivity:  $\sigma - \sigma_D = \Delta\sigma_{\text{SdH}} + \Delta\sigma_{\text{QPMR}}$ . The first term is proportional to Dingle factor  $\delta$  and describes SdH oscillations. It reads

$$\begin{aligned} \frac{\Delta\sigma_{\text{SdH}}}{\sigma_D} &= -4\delta \left\langle \cos\left(\frac{2\pi\epsilon}{\hbar\omega_c}\right) \right\rangle \cos\left(\frac{\pi\Delta_Z}{\hbar\omega_c}\right) \\ &= -4\delta A(T) \cos\left(\frac{2\pi\epsilon_F}{\hbar\omega_c}\right) \cos\left(\frac{\pi\Delta_Z}{\hbar\omega_c}\right), \end{aligned} \quad (5)$$

where  $\epsilon_F$  is Fermi energy and  $A(T) = \frac{(2\pi^2 kT/\hbar\omega_c)}{\sinh(2\pi^2 kT/\hbar\omega_c)}$  is the SdH temperature factor [1].

The second term is proportional to the square of the Dingle factor and describes variations of the conductivity due to QPMR. It reads

$$\begin{aligned} \frac{\Delta\sigma_{\text{QPMR}}}{\sigma_D} &= 4\delta^2 \left\langle \cos^2\left(\frac{2\pi\epsilon}{\hbar\omega_c}\right) \right\rangle \cos^2\left(\frac{\pi\Delta_Z}{\hbar\omega_c}\right) \\ &= \delta^2 \left[ 1 + \cos\left(\frac{2\pi\Delta_Z}{\hbar\omega_c}\right) \right]. \end{aligned} \quad (6)$$

In Eq. (6) the exponentially small temperature-dependent term is neglected. At  $\Delta_Z = 0$  Eq. (6) reproduces QPMR in perpendicular magnetic fields [18,25].

Equations (5) and (6) indicate the strong angular correlation between the amplitude of SdH oscillations and the QPMR. In particular the SdH amplitude is proportional to  $\cos(\pi\Delta_Z/\hbar\omega_c)$  and is zero at  $\Delta_Z = \hbar\omega_c/2$  in agreement with Eq. (1), while the QPMR is proportional to  $1 + \cos(2\pi\Delta_Z/\hbar\omega_c)$  and is zero too at  $\Delta_Z = \hbar\omega_c/2$ . In the next sections we compare experimental results with Eq. (5) and Eq. (6).

### B. Shubnikov de Haas oscillations

In quantizing magnetic fields  $\omega_c\tau_{tr} \gg 1$ , where  $\tau_{tr}$  is the transport scattering time. At this condition resistivity is  $\rho_{xx} = \sigma[\rho_{xy}]^2$  and  $\rho_{xx}(B_\perp)/\rho_0 = \sigma(B_\perp)/\sigma_D(B_\perp)$ , where  $\rho_0$  is Drude resistivity [24]. Therefore in accordance with Eq. (5) the amplitude of SdH oscillations of the normalized resistivity,  $\Delta\rho_{\text{SdH}}/\rho_0$ , is  $A_{\text{SdH}} = 4\delta A(T) \cos(\pi\Delta_Z/\hbar\omega_c)$ , and the normalized SdH amplitude is  $A_{\text{SdH}}^{\text{norm}} = A_{\text{SdH}}/[4\delta A(T)] = \cos(\pi\Delta_Z/\hbar\omega_c)$ . To extract the normalized amplitude  $A_{\text{SdH}}^{\text{norm}}$ , the SdH resistance oscillations shown in Fig. 1 were separated from the monotonic background using a low-frequency filtering [30]. The separated SdH oscillations were then divided by the factor  $4\rho_0\delta(B_\perp, \tau_q)A(T)$ . By a variation of the quantum scattering time  $\tau_q$  in the Dingle factor  $\delta$  quantum oscillations with the amplitude,  $A_{\text{SdH}}^{\text{norm}}$ , independent of the magnetic field,  $B_\perp$ , are obtained. The later indicates that the ratio of the Zeeman energy,  $\Delta_Z$ , to the cyclotron energy,  $\Delta_C = \hbar\omega_c$ , is a constant at fixed angle  $\alpha$  in the SdH regime. The insert to Fig. 2 shows the independence of the normalized SdH amplitude,  $A_{\text{SdH}}^{\text{norm}}$ , on the reciprocal magnetic fields at different angles  $\alpha$ .

Figure 2 presents the angular dependence of the normalized SdH amplitude  $A_{\text{SdH}}^{\text{norm}}$ . We note that the value of the SdH amplitude agrees quantitatively with the one expected from Eq. (5). The dependence is plotted versus  $\cos(\pi\Delta_Z/\hbar\omega_c) =$

$\cos[\pi mg/(2m_0 \cos\alpha)]$ . The  $g$  factor is used as a scaling parameter for  $x$  axes of the plot to provide the linear dependence between  $A_{\text{SdH}}^{\text{norm}}$  and  $\cos(\pi\Delta_Z/\hbar\omega_c)$ . The obtained value of  $g$  factor  $g = 0.97 \pm 0.08$  corresponds to the critical angle  $\alpha_c = 86.3^\circ \pm 0.3^\circ$  [see Eq. (1)] and is in a good agreement with existing experiments [7–10]. Thus the angular evolution of SdH oscillations agrees with both Eq. (5) and existing experiments. We note that the strong enhancement of the  $g$  factor obtained in the present experiments in the high-temperature regime is intriguing, since the enhancement should degrade with temperature increase in the low-temperature domain [8].

The obtained quantum scattering rate,  $1/\tau_q$ , is presented in Fig. 3(d). The scattering rate is found to be independent of the angle  $\alpha$ :  $1/\tau_q^{\text{SdH}} \approx 300 \pm 100$  GHz, and agrees with the one obtained using the QPMR described in next section.

### C. Quantum positive magnetoresistance

In accordance with Eq. (6) the magnitude of the quantum magnetoresistance decreases exponentially with the reciprocal magnetic field,  $1/B_\perp$ , due to the exponential decrease of Dingle factor  $\delta$ . Below we explore this property of the QPMR to extract the quantum scattering rate  $1/\tau_q$  and the normalized QPMR amplitude  $A_{\text{QPMR}}^{\text{norm}} = [1 + \cos(2\pi\Delta_Z/\hbar\omega_c)]/2$ . In the vicinity of the critical angle  $\alpha_c$  the magnitude of the QPMR is expected to be very small and the magnetoresistance should be mostly driven by other mechanisms [36–38]. In particular Fig. 3(b) presents the magnetoresistance at angle  $\alpha = 90^\circ$  at which only in-plane magnetic fields are applied. The resistance

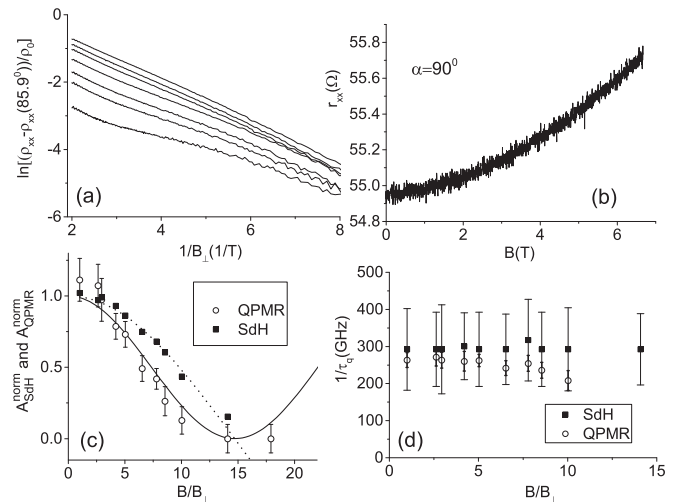


FIG. 3. (a) Dependence of the difference between normalized resistivity at an angle  $\alpha$  and the normalized resistivity at  $\alpha = 85.9^\circ \approx \alpha_c$ ,  $[\rho_{xx} - \rho_{xx}(85.9^\circ)]/\rho_0$ , on the reciprocal magnetic field. From the top curve to the bottom one corresponding angles  $\alpha$  are  $70.1, 76.2, 78.6, 81.2, 82.6, 83.3,$  and  $84.3$  degrees. (b) Magnetoresistance at  $\alpha = 90^\circ$ . (c) Dependence of the normalized QPMR and SdH amplitudes on the ratio between total and perpendicular magnetic fields. The solid (dotted) line presents the normalized QPMR (SdH) amplitude,  $A_{\text{QPMR}}^{\text{norm}} = [1 + \cos(2\pi\Delta_Z/\hbar\omega_c)]/2$  ( $A_{\text{SdH}}^{\text{norm}}$ ), obtained from Eq. (6) [Eq. (5)] using  $g$  factor  $g = 0.97$ . (d) Dependence of the quantum scattering rate on the ratio  $B/B_\perp$  obtained from the analysis SdH oscillations and the exponential decrease of the QPMR magnitude with  $1/B_\perp$  expected from Eq. (6).

demonstrates a weak (within 2%) parabolic increase with the in-plane magnetic field. The small in-plane magnetoresistance affects weakly the curves presented in Fig. 1 and can be taken into account assuming its independence on the angle  $\alpha$ . Below we assume that all mechanisms leading to negative magnetoresistance in the vicinity of the critical angle are independent of the angle  $\alpha$  and controlled by  $B_{\perp}$  and  $B_{\parallel}$  independently.

Within this assumption the difference between magnetoresistance at an angle  $\alpha$  and the magnetoresistance at the critical angle  $\alpha_c$  captures the main effect of the angular variations of the electron spectrum on the electron transport described by Eq. (6). Figure 3(a) presents the dependence of the difference between the resistivity  $\rho_{xx}(\alpha)$  and  $\rho_{xx}(85.9^{\circ} \approx \alpha_c)$  normalized to the Drude resistivity  $\rho_0$  on the reciprocal magnetic field,  $1/B_{\perp}$ , taken at different angles. At small magnetic fields,  $B_{\perp}$ , the dependencies demonstrate an exponential decrease with  $1/B_{\perp}$  in accord with Eq. (6) with the rate depending weakly on  $\alpha$ . With an increase of the angle  $\alpha$  the dependencies shift down indicating a decrease of the normalized QPMR amplitude  $A_{QPMR}^{\text{norm}}$ . The presented resistance difference takes into account the small variations of the resistivity with the in-plane magnetic field shown in Fig. 3(b). The applied correction to the resistivity affects very weakly (within the size of the symbols) the results presented in Figs. 3(c) and 3(d).

Figure 3(c) presents the normalized QPMR amplitude  $A_{QPMR}^{\text{norm}}$  and SdH amplitude  $A_{SdH}^{\text{norm}}$  plotted vs  $1/\cos \alpha = B/B_{\perp}$ . The normalized QPMR amplitude is obtained by the extrapolation of the linear dependencies shown in Fig. 3(a) at high  $1/B_{\perp}$  to the infinite  $B_{\perp}$ . The extracted normalized amplitude  $A_{QPMR}^{\text{norm}}$  is presented by the open symbols. The solid line shows the amplitude  $A_{QPMR}^{\text{norm}}$  obtained from Eq. (6) using  $g$  factor  $g = 0.97$ . We note that there are no fitting parameters between the experiment (open symbols) and the Eq. (6) since the  $g$  factor is obtained from the fitting of the angular dependence of the SdH amplitude. Shown in Fig. 3(c) comparison of two amplitudes indicates strong angular correlations between SdH resistance oscillations and the quantum positive magnetoresistance.

Figure 3(d) presents the quantum scattering rates obtained from the analysis of SdH resistance oscillations (filled symbols) and QPMR (open symbols). In contrast to SdH resistance oscillations the analysis of the QPMR magnitude yields more accurate results for  $\tau_q$  since QPMR does not depend on the temperature damping factor  $A(T)$  and the response is mostly controlled by the Dingle factor only. The quantum scattering rates extracted by two different methods are found to be in a reasonable agreement indicating no significant variations of the electron lifetime  $\tau_q$  with both the angle  $\alpha$  and the applied magnetic fields at  $\alpha < \alpha_c$ .

Figures 1 and 3(a) demonstrate the evolution of the QPMR, which is obtained at a fixed angle  $\alpha$ . At this condition both perpendicular and total magnetic fields are changing. As mentioned above the angular evolution of QPMR at small ( $< 65^{\circ}$ ) and large ( $> \alpha_c$ ) angles demonstrates additional features, which may require a modification of the proposed description. To get further insight into the angular evolution of the QPMR, we have conducted measurements at a fixed perpendicular magnetic field,  $B_{\perp}$ , while sweeping the in-plane magnetic field,  $B_{\parallel}$ . At this condition the cyclotron energy is

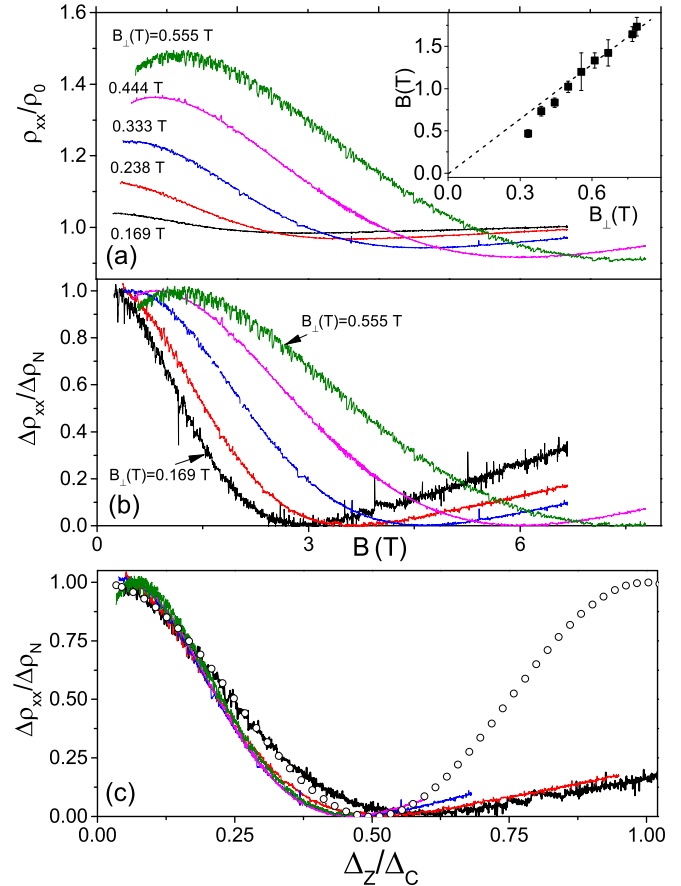


FIG. 4. (a) Dependence of normalized resistivity on magnetic field at fixed  $B_{\perp}$  as labeled. Inset shows position of the resistance maximum at different  $B_{\perp}$ . (b) Normalized variations of the resistivity shown in (a):  $\Delta\rho_{xx}/\Delta\rho_N = (\rho_{xx} - \rho_{\min})/(\rho_{\max} - \rho_{\min})$  vs  $B$ . (c) Normalized variations of the resistivity vs ratio of Zeeman and cyclotron energies,  $\mu g B/\hbar\omega_c$ , with  $g$  factor  $g = 0.97$  obtained from the angular variation of SdH oscillations. Open symbols present the normalized magnetoresistance expected from Eq. (6) with no fitting parameters.

fixed and variations of the electron spectrum are related mostly to spin degrees of freedom.

Figure 4(a) presents dependencies of the normalized resistivity on the total magnetic field taken at the fixed  $B_{\perp}$  as labeled. In the agreement with the angular evolution shown in Fig. 1 the total magnetic field suppresses the quantum magnetoresistance at a fixed  $B_{\perp}$ . A stronger perpendicular magnetic field,  $B_{\perp}$ , requires a stronger total magnetic field,  $B$ , to suppress the QPMR. After the suppression the magnetoresistance demonstrates a weak increase with the magnetic field, which is, however, much smaller than expected from Eq. (6). Finally at  $B_{\perp} > 0.3$  T the magnetoresistance shows a maximum enhancing at higher  $B_{\perp}$  that is also not explained by this model. The inset to Fig. 4(a) presents the position of the resistance maximum at different  $B_{\perp}$  indicating that the maximum occurs at  $\alpha_0 \approx 62^{\circ}$ .

Figure 4(b) presents the magnetic field dependencies of a normalized resistance variation:  $\Delta\rho_{xx}/\Delta\rho_N = (\rho_{xx} - \rho_{\min})/(\rho_{\max} - \rho_{\min})$ , where  $\rho_{\max}$  and  $\rho_{\min}$  are maximum and minimum values of the curves shown in (a). The figure

facilitates the comparison of the shape of the dependencies at different  $B_{\perp}$ .

In accordance with the proposed model [see Eq. (6)] at a fixed  $B_{\perp}$  and a constant quantum lifetime  $\tau_q$  the Dingle factor is fixed and the evolution of the magnetoresistance is solely due to variations of the QPMR amplitude,  $A_{QPMR}^{\text{norm}} = [1 + \cos(2\pi \Delta_Z / \hbar \omega_c)]/2$ . If the  $g$  factor is also a constant, then the Zeeman term,  $\Delta_Z = \mu g B$ , is linearly proportional to the total magnetic field,  $B$ , and the QPMR amplitude depends only on the ratio  $B/B_{\perp}$ . Thus in this case the QPMR should scale with  $B/B_{\perp}$ .

Figure 4(c) presents the normalized resistance variations,  $\Delta\rho_{xx}/\Delta\rho_N$ , shown in Fig. 4(b) plotted against the ratio between Zeeman and cyclotron energies:  $\Delta_Z/\Delta_C = (mg/2m_0)(B/B_{\perp})$ , using the constant  $g$  factor  $g = 0.97$  obtained from the angular dependence of the amplitude of SdH oscillations. Except for the curve taken at the smallest  $B_{\perp} = 0.169$  T all other curves shown in Figs. 4(a) and 4(b) collapse on a single dependence at  $\Delta_Z/\Delta_C$  between 0.07 and 0.5. The collapse indicates  $B/B_{\perp}$  scaling, which holds at high  $B_{\perp}$  in the studied system.

At  $\Delta_Z/\Delta_C < 1/2$  the scaled dependencies are quite close to the dependence expected from Eq. (6) and presented by the open circles at  $g = 0.97$  in Fig. 4(c) with no fitting parameters. The dependence obtained at the smallest  $B_{\perp} = 0.169$  T agrees better with the model. We note that the model takes into account only fundamental harmonics of the electron spectrum and, thus, is valid only for overlapping Landau levels at  $\omega_c \tau_q < 1$ . At  $B_{\perp} > 0.3$  T the Landau levels become separated at  $\tau_q \approx 4$  ps and an account of the higher harmonics of DOS may improve the agreement with the experiment at high  $B_{\perp}$ . In contrast the description of SdH oscillations is valid even at higher  $B_{\perp}$  since the contributions of the higher harmonics of DOS to the SdH amplitude are suppressed by the temperature for presented  $B_{\perp}$  [1,25]. We note also that the shift of the resistive variation at  $B_{\perp} = 0.169$  T to a stronger  $B$  ( $\Delta_Z$ ) in Fig. 4(c) agrees with the reduction of the enhanced  $g$  factor by the disorder [8,17].

An unexpected feature of the dependencies presented in Fig. 4 is the resistance maximum emerging at high  $B_{\perp}$ . In accordance with Eq. (6) the maximum occurs at  $\Delta_Z = 0$  and corresponds to the alignment of the quantum levels corresponding to spin-up and spin-down subbands. The presence of the maximum at a finite magnetic field,  $B$ , suggests that the magnitude of the Zeeman splitting,  $|\Delta_Z(B_{\perp})|$ , decreases with the increase of the total magnetic field,  $B$ , at a small  $B_{\parallel}$ . The decrease of the spin splitting is stronger at larger  $B_{\perp}$ . The total magnetic field,  $B_{\text{max}}$ , corresponding to the resistance maximum at different  $B_{\perp}$  is shown in the inset to Fig. 4(a). At high  $B_{\perp}$  the  $B_{\text{max}}$  is proportional to  $B_{\perp}$  that corresponds to the angle  $\alpha_0 = 62^\circ$ . The position of the maximum agrees, therefore, with the  $B/B_{\perp}$  scaling.

The observed behavior is compatible with the following relation between an effective spin splitting  $\Delta_{\text{spin}}$  and magnetic fields:

$$\Delta_{\text{spin}} = \mu|g|B + \Delta_{\perp}, \quad \Delta_{\perp} = \beta\hbar\omega_c, \quad (7)$$

where  $\beta < 0$ . The parameter  $\Delta_{\perp}$  describes the additional contribution of the perpendicular magnetic field to the spin

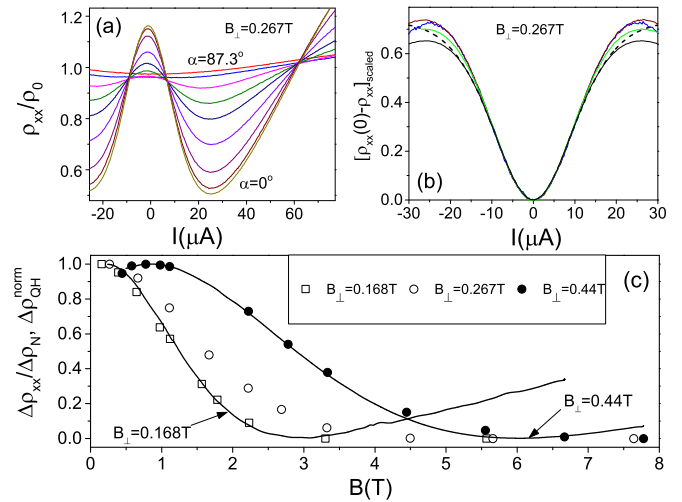


FIG. 5. (a) Quantal heating of 2D electrons at different angles  $\alpha$ : 0, 66.4, 76.1, 80.8, 83.1, 84.3, 85.4, 86.6, 87.3 degrees at  $B_{\perp} = 0.267$  T. (b) Solid lines are variations of the resistance shown in (a), scaled vertically by factor  $k(\alpha)$ , vs the electric current  $I$  at several angles  $\alpha = 0, 76.1, 80.8,$  and  $84.3$ . Dashed line presents fit, which follows from Eq. (8) for the differential resistance [39]. (c) Solid curves present smoothed dependencies of the normalized variations of the resistance  $\Delta\rho_{xx}/\Delta\rho_N$  on the magnetic field  $B$ . Symbols present the normalized magnitude of the heating induced resistance variation,  $\Delta_{QH}^{\text{norm}} = k(\alpha)/k_{\text{max}}$ , obtained at different magnetic fields  $B_{\perp}$  and  $B$  as labeled.

splitting. At the resistance maximum  $\Delta_{\text{spin}} = 0$  yielding  $\beta = -m|g| \cos \alpha_0 / (2m_0) \approx -0.016|g|$ .

The structure of the effective spin splitting in Eq. (7) is similar to the one used for 2D electron systems [8,10]. In particular in Eq. (10) of Ref. [8],  $\Delta_{\text{spin}} = \mu g B + \gamma \hbar \omega_c$ , the second term proportional to  $B_{\perp}$  is the contribution from electron-electron interaction [3,15]. The important difference is, however, that the sign of the second term,  $\gamma \hbar \omega_c$ , is opposite to the sign of the term  $\Delta_{\perp}$  in Eq. (7). Furthermore the magnitude of the  $\beta$  is an order of magnitude smaller the  $\gamma \approx 0.2$ . The origin of these maxima requires further investigations.

At  $\Delta_Z/\Delta_C > 1/2$  the angular evolution of the QPMR deviates significantly from the expected behavior. Instead of periodic oscillations with the parameter  $\Delta_Z/\Delta_C$  the resistance demonstrates a weak increase at angles  $\alpha > 86^\circ$  indicating that the modulation of the density of states with the energy does not evolve as expected from Eq. (6). Accounting for the magnetoresistance due to the in-plane magnetic field [presented in Fig. 3(b)] reduces this resistance increase at  $\Delta_Z/\Delta_C > 1/2$  further (not shown).

To get a better understanding of the DOS at  $\Delta_Z/\Delta_C > 1/2$  we have conducted measurements of quantal heating [19–21]. Figure 5(a) presents dependencies of the normalized differential resistance on the electric current obtained at fixed  $B_{\perp}$  and different total magnetic fields  $B = B_{\perp}/\cos \alpha$ . An application of dc current decreases considerably the differential resistance due to quantal heating. In accordance with theory the magnitude of the heating induced variation of the conductivity at small perpendicular magnetic fields is propor-

tional to the square of the magnitude of DOS modulations with the energy:  $2\delta^2$  [35]. Using Eq. (2) for the DOS and Eq. (4) for the conductivity one can find the effect of quantal heating on the conductivity in a tilted magnetic field following the case corresponding to  $\alpha = 0^\circ$  and considering the inelastic relaxation in the  $\tau$  approximation [35]. The variation of the conductivity due to quantal heating,  $\Delta\sigma_{QH} = \sigma(I) - \sigma(0)$ , at  $\omega_c\tau_q < 1$  is the following:

$$\frac{\Delta\sigma_{QH}}{\sigma_D} = -\delta^2 \left[ 1 + \cos\left(\frac{2\pi\Delta_Z}{\hbar\omega_c}\right) \right] \frac{4Q_{dc}}{1+Q_{dc}}. \quad (8)$$

The term  $Q_{dc} = [2\tau_{in}/\tau_{tr}][eER_c]^2[\pi/\omega_c]^2$ , where  $\tau_{in}$  ( $\tau_{tr}$ ) is inelastic (transport) time,  $R_c$  is cyclotron radius, and  $E \sim I$  is the electric (Hall) field [35,39]. Equation (8) follows from Eq. (15) of Ref. [35] if one substitutes the factor  $2\delta^2$  by  $\delta^2[1 + \cos(2\pi\Delta_Z/\hbar\omega_c)]$ . Equation (8) indicates that the magnitude of the conductivity variation at different angles depends on the factor  $[1 + \cos(2\pi\Delta_Z/\hbar\omega_c)]$ , which is identical to the one describing QPMR magnitude [see Eq. (6)]. On the other hand the factor  $Q_{dc}/(1+Q_{dc})$ , describing variations of the resistance with the electric field (current), does not depend on the angle  $\alpha$ . This means that the shape of the current dependence of the resistance is expected to be the same at different angles, while the overall magnitude of the resistance variations should depend of the angle.

Figure 5(b) demonstrates that the heating-induced resistance variations,  $\rho_{xx}(0) - \rho_{xx}(I)$ , at different angles  $\alpha$  are indeed proportional to each other and to the one expected from Eq. (8) [39]. To reveal the proportionality the curves, shown in Fig. 5(a), are scaled vertically to follow the same dependence on the applied current,  $I$ . At high currents the dependencies deviate from the theory due to other mechanisms of nonlinearity [19].

The normalized magnitude of the heating-induced resistance variation  $\Delta Q_{QH}^{\text{norm}} = k(\alpha)/k_{\text{max}}$  is shown in Fig. 5(c) at different  $B$  and  $B_\perp$ . Here  $k(\alpha)$  is the reciprocal scaling coefficients of the curves in Fig. 5(b) and  $k_{\text{max}}$  is the maximum value of  $k$ . At  $\Delta_Z/\Delta_C < 1/2$  the heating-induced resistance variations follow the QPMR magnitude in agreement with Eq. (6) and Eq. (8) and, thus, correlate with the angular variations of the SdH amplitude. The latter is in agreement with previous observations [21]. At  $\Delta_Z/\Delta_C > 1/2$  the heating-induced resistance variations are absent, indicating the absence of oscillations of the DOS in this regime. On another hand at  $\Delta_Z/\Delta_C < 1/2$  the angular evolution of SdH oscillations, QPMR, and quantal heating indicates quantization of the electron spectrum demonstrating the electron lifetime  $\tau_q \approx 4$  ps independent of the angle  $\alpha$ .

The results show, thus, a rather abrupt transition of the quantized electron spectrum at  $\Delta_Z/\Delta_C < 1/2$  to an uniform, energy-independent DOS at  $\Delta_Z/\Delta_C > 1/2$ . Both these results and investigations of the angular evolution of SdH oscillations [8,10], thus, do not support the proposal of a gradual decrease of the quantum scattering time with the in-plane magnetic field [40,41]. The observed quenching of microwave-induced resistance oscillations in tilted magnetic fields [41–43] also indicates a modification of the electron spectrum, which happens, however, at smaller angles  $\alpha < \alpha_c$ . This suggests that the transition to an energy-independent DOS in the

high-temperature regime,  $kT \gg \hbar\omega_c$ , may depend not only on the ratio between Zeeman and cyclotron energies but also on some other parameters such as electron density, disorder [17], and/or the width of the quantum well.

The angular evolution of QPMR indicates significant spin mixing. This spin mixing suggests an important role of the spin-orbit coupling in electron transport at high filling factors. The importance of spin-orbit interaction for the quantized spectrum increases at small magnetic fields since the strength of this interaction is independent of magnetic field [22,23]. The observed absence of QPMR and quantal heating at  $\Delta_Z/\Delta_C > 1/2$  suggests a transition of the quantized electron orbital motion and the independent periodic spin evolution to a stochastic spin-orbital dynamics when energy (period) of the spin evolution is compatible with the energy (period) of the orbital motion. Below we evaluate the effect of spin-orbit interaction on spin mixing in the studied system.

#### D. Spin-orbit interaction and quantum positive magnetoresistance

Spin-orbit coupling in quantum wells and heterojunctions has been discussed in the literature [4]. In particular the significant deviation of the  $g$  factor obtained in electrically detected electron spin resonance (ESR) from the bulk GaAs value [11] has been attributed to spin-orbit effects [23]. The spin-orbit interaction leads to positive quantum corrections to conductivity of disordered 2D conductors [44–46]. In GaAs heterojunctions the effect of spin-orbit interaction on quantum corrections to the conductivity has been investigated [47,48].

We consider that the spin mixing leading to QPMR is due to impurity scattering between different  $s$  sectors of the Hamiltonian (9) containing a spin-orbit interaction. To evaluate the spin mixing we first find the electron spectrum, then compute numerically matrix elements of the impurity-induced transitions both within an  $s$  sector and between different  $s$  sectors and compare them.

We consider a 2DEG in the  $x$ - $y$  plane placed in a tilted magnetic field and affected by a Rashba spin-orbit term [22,23,49]. The in-plane component of the magnetic field is chosen to be along the  $x$  direction yielding  $\mathbf{B} = (B_\parallel, 0, B_\perp)$ . The Hamiltonian of the system can be written in the following form:

$$H = \frac{1}{2m} \left( \mathbf{p} + \frac{e}{c} \mathbf{A} \right)^2 + \frac{\lambda}{\hbar} \hat{\mathbf{z}} \cdot \left[ \left( \mathbf{p} + \frac{e}{c} \mathbf{A} \right) \times \boldsymbol{\sigma} \right] + \frac{1}{2} \mu_B g B_\perp \sigma_z + \frac{1}{2} \mu_B g B_\parallel \sigma_x, \quad (9)$$

where  $m$ ,  $-e$ , and  $\lambda$  are the electron mass, charge, and spin-orbit coupling constant, respectively, and  $\sigma_i$  are the Pauli matrices. We employ Landau gauge  $\mathbf{A} = -yB\hat{\mathbf{x}}$ . In that case the Hamiltonian does not contain the  $x$  variable and the momentum in the  $x$  direction  $p_x = \hbar k$  is a conserved quantity.

As was noted previously [49] at angle  $\alpha = 0$  the problem can be solved analytically yielding the following energy

spectrum [22,23]:

$$E_{n,s} = \hbar\omega_c \left( n + \frac{s}{2} \sqrt{(1-g_s)^2 + 8\eta^2 n} \right), \quad (10)$$

where  $\eta = \lambda m l_B / \hbar^2$  and  $g_s = gm/2m_0$ . Here  $l_B = \sqrt{\hbar/eB_\perp}$  is the magnetic length. In Eq. (10)  $s = 1$  for  $n = 0$  and  $s = \pm 1$  for  $n > 0$ . We note that at  $\lambda = 2.5$  meV nm obtained from an analysis of the ESR spectrum in GaAs heterojunctions [11,23] the spin-orbital term,  $8\eta^2 n$ , provides a significant contribution to the gap between different  $s$  sectors in Eq. (10) at the high filling factors ( $n \sim 30$ ) relevant to the experiments.

The corresponding eigenfunctions have the form

$$\psi_{n,k,s}(x,y) = \cos \theta_{n,s} \chi_{n,k,+1} + i \sin \theta_{n,s} \chi_{n-1,k,-1}, \quad (11)$$

where  $\theta_{0,1} = 0$  and for  $n > 0$ ,  $\tan \theta_{n,s} = -u_n + s\sqrt{u_n^2 + 1}$  and  $u_n = (1-g_s)/(\eta\sqrt{8n})$ . Functions  $\chi_{n,k,\sigma} = \phi_{n,k}|\sigma\rangle$  present the eigenfunctions of the Hamiltonian (9) at  $\lambda = 0$  and  $B_{\parallel} = 0$ , where  $\phi_{n,k}$  are the Landau level eigenfunctions and  $|\sigma\rangle$  is the eigenstate of the spin operator  $\sigma_z$  with eigenvalues  $\sigma = \pm 1$ . Each eigenstate  $\psi_{n,k,s}$  has the degeneracy  $N_\phi = L_x L_y eB / (\hbar c)$  related to  $N_\phi$  values of  $k$ , where  $L_x$  and  $L_y$  are the system sizes in the  $x$  and  $y$  directions, respectively.

In a tilted magnetic field,  $\alpha > 0$ , the problem can be solved numerically [49]. An application of the in-plane magnetic field,  $B_{\parallel}$ , induces transitions between states  $\psi_{n,k,s}$  with different index  $s$  (between different  $s$  sectors). Using functions  $\psi_{n,k,s}$  as the basis set, one can present the Hamiltonian in matrix form [30]. The matrix contains four matrix blocks:  $\hat{H} = (\hat{E}^+, \hat{T}; \hat{T}^*, \hat{E}^-)$ , where the semicolon separates rows. The diagonal matrices  $\hat{E}^+$  and  $\hat{E}^-$  represent energy of the  $s$  sectors with  $s = 1$  and  $s = -1$ , respectively, in different orbital states  $n$  following Eq. (10):

$$E_{nm}^+ = \delta_{nm} \hbar\omega_c \left( (n-1) + \frac{1}{2} \sqrt{(1-g_s)^2 + 8\eta^2(n-1)} \right), \quad (12)$$

$$E_{nm}^- = \delta_{nm} \hbar\omega_c \left( n - \frac{1}{2} \sqrt{(1-g_s)^2 + 8\eta^2 n} \right),$$

where indexes  $n = 1, 2, \dots, N_{\max}$  and  $m = 1, 2, \dots, N_{\max}$  enumerate rows and columns of the matrix correspondingly. In numerical computations the maximum number  $N_{\max}$  is chosen to be about 2 times larger than the orbital number  $N_F$  corresponding to Fermi energy  $E_F$ . Further increase of  $N_{\max}$  shows a very small (within 1%) deviation from the dependencies obtained at  $N_{\max} \approx 2N_F$ .

The corresponding matrix elements of the off-diagonal matrix  $\hat{T}$  are the following:

$$T_{nm} = i \delta_{nm} \frac{\mu_B g B_{\parallel}}{2} \cos \theta_{n-1,1} \sin \theta_{m,-1}. \quad (13)$$

The Hamiltonian  $\hat{H}$  is diagonalized numerically at different magnetic fields  $B_\perp$  and  $B_{\parallel}$ . To analyze the spectrum the obtained eigenvalues of the Hamiltonian are numerated in ascending order using positive integer index  $l = 1, 2, \dots$ . The electron transport depends on the distribution of the quantum levels in the interval  $kT$  near the Fermi energy  $E_F$  [24]. Below we focus on this part of the spectrum.

Figure 6 presents the difference between energies of the  $(l+1)$ th and  $l$ th quantum levels of the electron spectrum.

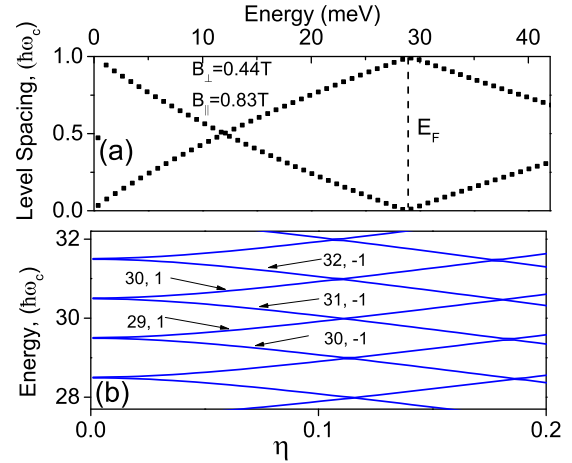


FIG. 6. (a) Level spacing  $\delta E_l = E_{l+1} - E_l$  in the energy spectrum of electrons in  $B_\perp = 0.44$  T and  $B_{\parallel} = 0.83$  T at spin-orbit coupling  $\lambda = 2.95$  meV nm and  $g = -0.44$ . (b) Dependence of the energy of the quantum states in the vicinity of Fermi energy on the spin-orbit coupling parameter  $\eta$  at  $B_\perp = 0.44$  T and  $\alpha = 0^\circ$ . Labels show quantum indexes of the levels according to Eq. (10).

Each symbol represents a particular level spacing normalized to the cyclotron energy:  $\delta E_l / \hbar\omega_c = (E_{l+1} - E_l) / \hbar\omega_c$  [30]. Figure 6(a) presents the normalized level spacing at spin-orbit coupling  $\lambda = 2.95$  meV nm and  $g = -0.44$  obtained in  $B_\perp = 0.44$  T and  $B_{\parallel} = 0.83$  T. These magnetic fields correspond to the QPMR maximum shown in Fig. 4. At these conditions the two nearest quantum levels coincide in the vicinity of Fermi energy,  $E_F$ , yielding the level splitting  $\Delta^* = 0$ . Figure 6(b) presents the energy of the quantum levels in the vicinity of the Fermi energy vs the strength of the spin-orbit coupling characterized by the coefficient  $\eta$  at  $B_\perp = 0.44$  T and  $\alpha = 0^\circ$ . Near  $\eta \approx 0.11$  the levels of two different  $s$  sectors intersect opening a channel for the impurity scattering between  $s$  sectors. Below we evaluate the rate of these transitions for the crossing of the level with quantum numbers  $n_0 = 30$ ,  $s = 1$  and the one with  $n_0 + 2 = 32$ ,  $s = -1$  and investigate the relation of the scattering matrix elements inside the same  $s$  sector and between different  $s$  sectors.

We approximate the impurity potential by a Gaussian function located at the  $(0,0)$  point:

$$V(x,y) = V_0 \exp \left[ -\frac{x^2 + y^2}{2a^2} \right], \quad (14)$$

where  $V_0$  is the amplitude of the impurity potential and  $a$  defines its width. For very narrow impurity potential Eq. (14) can be reduced to a delta function  $V_D(x,y) = 2\pi V_0 a^2 \delta(x)\delta(y)$ . In this case at  $\alpha = 0^\circ$  the matrix elements can be written explicitly:

$$\begin{aligned} \langle n,s,k | V_D(x,y) | n',s',k' \rangle \\ = 2\pi V_0 a^2 \times [\sin \theta_{n,s} \sin \theta_{n',s'} \phi_{n-1,k}(0,0) \phi_{n'-1,k'}(0,0) \\ + \cos \theta_{n,s} \cos \theta_{n',s'} \phi_{n,k}(0,0) \phi_{n',k'}(0,0)], \end{aligned} \quad (15)$$

whereas for the general case they should be computed numerically.

Below we compute the matrix elements inside the same  $s$  sector  $\langle n_0, 1, k | V(x,y) | n_0, 1, k' \rangle$  and between different sectors

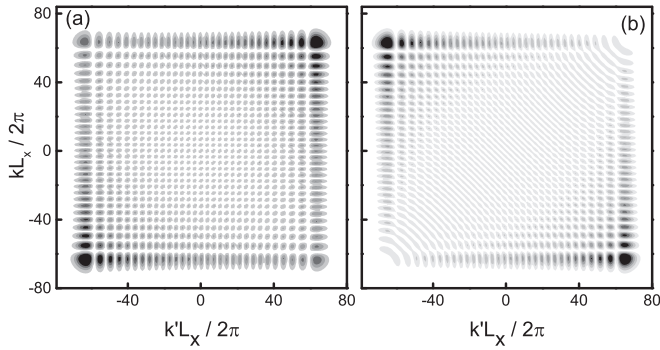


FIG. 7. The contour plots of  $|\langle n_0, 1, k | V(x, y) | n_0, 1, k' \rangle|$  (a) and  $|\langle n_0, 1, k | V(x, y) | n_0 + 2, -1, k' \rangle|$  (b) for different values of  $k$  and  $k'$  for Gaussian impurity potential with parameters  $V_0 = 0.1\hbar\omega_c$ ,  $a = 6.6 \times 10^{-4}l_B$ , and  $\eta \approx 0.11$ .

$\langle n_0, 1, k | V(x, y) | n_0 + 2, -1, k' \rangle$  at the value  $\eta \approx 0.11$  and compare the magnitudes of these two matrix elements. In calculations the size of the system in the  $y$  direction is  $L_y = 6R_c$ , where  $R_c = \sqrt{2n_0 + 1}l_B$  is the cyclotron radius.

Figure 7(a) shows a contour plot of the magnitude of the matrix element  $|\langle n_0, 1, k | V(x, y) | n_0, 1, k' \rangle|$  within the same  $s$  sector while Fig. 7(b) shows the magnitude of the impurity scattering between different  $s$  sectors  $|\langle n_0, 1, k | V(x, y) | n_0 + 2, -1, k' \rangle|$  for different values of  $k$  and  $k'$ . The impurity parameters are  $V_0 = 0.1\hbar\omega_c$  and  $a = 6.6 \times 10^{-4}l_B$ . Figure 7(a) demonstrates that for scattering within the same sector both forward scattering ( $k = k'$ ) and backscattering ( $k = -k'$ ) are substantial, although forward scattering is somewhat stronger than backscattering. In contrast, in transitions between different  $s$  sectors backscattering plays the major role while forward scattering is strongly suppressed. The average of the squares of scattering amplitudes is found to be of the same order:  $1.22 \times 10^{-19}(\hbar\omega_c)^2$  within the same  $s$  sector and  $0.72 \times 10^{-19}(\hbar\omega_c)^2$  between different  $s$  sectors. Thus due to backscattering the impurity scattering between different  $s$  sectors is comparable with that within the same  $s$  sector. We note that the studied systems demonstrate a significant magnitude of impurity backscattering [50–52].

Figure 8(a) presents the dependence of the averaged square of the matrix elements on the shape of the impurity potential  $V(x, y)$  at  $\eta \approx 0.11$ . The average is over all  $k$  and  $k'$  values. This figure shows that at  $a < 0.05l_B$  both Gaussian and delta function potentials provide nearly identical scattering both within the  $s$  sector and between different  $s$  sectors and the scattering magnitude is proportional to the cross section of the impurity potential  $a^2$ . At higher magnetic fields  $a > 0.05l_B$  the scattering on the Gaussian potential deviates from the  $a^2$  dependence. More importantly the figure shows that at  $a > 0.05l_B$  the impurity potential cannot provide significant scattering between different  $s$  sectors. Thus the scattering between different  $s$  sectors is effective at relatively small magnetic fields (high filling factors) and/or for sharp impurities. At the upper limit of the perpendicular magnetic fields used in this study,  $B_\perp \approx 1$  T, the magnetic length  $l_B \approx 25$  nm and for impurities with size  $a$  less 1 nm backscattering is effective and leads to the strong spin mixing at  $B_\perp < 1$  T. The size,  $a < 1$  nm, is reasonable for neutral impurities in a solid.

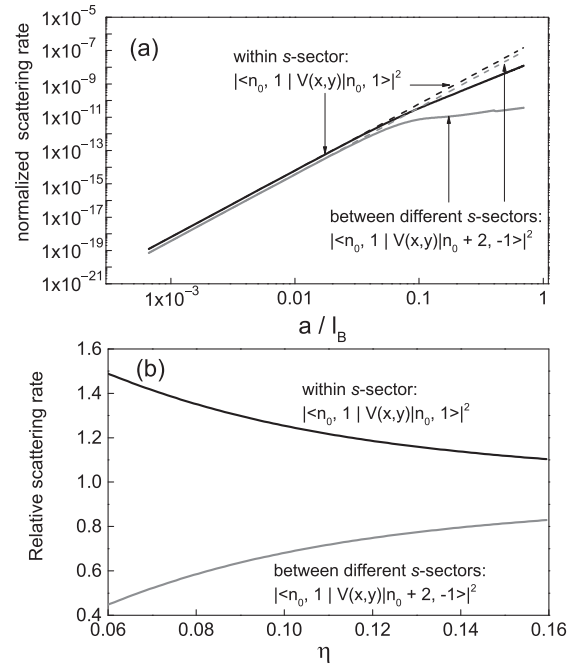


FIG. 8. (a) The dependence of the square of matrix elements on impurity width parameter  $a$  both for Gaussian  $V(x, y)$  and delta  $V_D(x, y)$  function potential cases for  $\eta \approx 0.11$ . (b) The dependence of the square of matrix elements on the value of spin-orbit interaction parameter  $\eta$  for Gaussian impurity with the width parameter  $a = 6.6 \times 10^{-4}l_B$ . The impurity amplitude is  $V_0 = 0.1\hbar\omega_c$  for both figures and the amplitudes of matrix elements are averaged over all  $k$  and  $k'$  values.

Due to the impurity scattering quantum levels are broadened and the elastic transitions may occur in an interval of the energies when two levels overlap. Thus the scattering may exist in an interval of the parameter  $\eta$ . Figure 8(b) presents the dependence of the averaged square of matrix elements on the parameter  $\eta$ . The  $\eta$  is varied in the range, where the energy of the system changes by about  $0.6\hbar\omega_c$ . It accounts, thus, for a significant broadening of quantum levels. The figure shows that the amplitudes of both the intrasector and intersector scattering are quite comparable in the broad range of  $\eta$  and the difference decreases with the  $\eta$  increase. The increase of the scattering between different  $s$  sectors is related to the fact that at  $\eta = 0$  different sectors correspond to eigenstates with different  $z$  components of the electron spin. These states cannot be coupled by the impurity scattering unless a magnetic impurity is involved [see Eq. (15)]. Due to the fact that the majority of the impurities in the studied systems are nonmagnetic the scattering between different sectors is completely mediated by the spin-orbit interaction and increases with the increase of the spin-orbit coupling.

The presented estimations of the impurity scattering in the presence of spin-orbit interaction indicate that in the range of physical parameters relevant to presented experiments the scattering between different  $s$  sectors is comparable with the scattering within the same  $s$  sector. This leads to strong spin mixing in the studied systems and, thus, supports the assumption used for Eq. (3).

#### IV. CONCLUSION

Quantum positive magnetoresistance (QPMR) of 2D electrons is studied at different angles  $\alpha$  between the magnetic field and the normal to the 2D layer. The magnitude of QPMR varies significantly with the magnetic field tilt. The angular evolution of QPMR correlates strongly with angular variations of the amplitude of SdH resistance oscillations indicating that the Zeeman spin splitting,  $\Delta_Z$ , enhanced by electron-electron interaction, is the dominant mechanism leading to the QPMR reduction. Surprisingly no quantization of the electron spectrum is detected when the Zeeman energy exceeds half of the cyclotron energy suggesting a transformation of the electron dynamics in the high-temperature regime at  $kT \gg \Delta_Z > \hbar\omega_c/2$ .

In contrast to SdH oscillations the angular evolution of QPMR implies substantial mixing between spin subbands. Spin mixing has been detected in other 2D electron systems [31,32]. Although the origin of the spin mixing remains puzzling investigations indicate that the spin-orbit interaction may lead to significant spin mixing via impurity scattering in the studied system.

#### ACKNOWLEDGMENTS

This work was supported by the National Science Foundation (Division of Material Research, 1104503), the Russian Foundation for Basic Research (Project No. 14-02-01158), and the Ministry of Education and Science of the Russian Federation. We also acknowledge support from NSF EFRI 1542863 (A.G. and P.G.).

- 
- [1] D. Shoenberg, *Magnetic Oscillations in Metals* (Cambridge University Press, New York, 1984).
- [2] S. D. Sarma and A. Pinczuk, *Perspectives in Quantum Hall Effects* (Wiley-VCH, Weinheim, 2004).
- [3] T. Ando, A. B. Fowler, and F. Stern, *Rev. Mod. Phys.* **B 54**, 437 (1982).
- [4] M. I. Dyakonov, editor, *Spin Physics in Semiconductors* (Springer-Verlag, Berlin, 2008).
- [5] A. B. Fowler, F. F. Fang, W. E. Howard, and P. J. Stiles, *Phys. Rev. Lett.* **16**, 901 (1966).
- [6] F. F. Fang and P. J. Stiles, *Phys. Rev.* **174**, 823 (1968).
- [7] R. J. Nicholas, R. J. Haug, K. v. Klitzing, and G. Weimann, *Phys. Rev. B* **37**, 1294 (1988).
- [8] D. R. Leadley, R. J. Nicholas, J. J. Harris, and C. T. Foxon, *Phys. Rev. B* **58**, 13036 (1998).
- [9] B. A. Piot, D. K. Maude, M. Henini, Z. R. Wasilewski, J. A. Gupta, K. J. Friedland, R. Hey, K. H. Ploog, U. Gennser, A. Cavanna, D. Mailly, R. Airey, and G. Hill, *Phys. Rev. B* **75**, 155332 (2007).
- [10] A. T. Hatke, M. A. Zudov, L. N. Pfeiffer, and K. W. West, *Phys. Rev. B* **85**, 241305(R) (2012).
- [11] D. Stein, K. V. Klitzing, and G. Weimann, *Phys. Rev. Lett.* **51**, 130 (1983).
- [12] Yu. A. Nefyodov, A. V. Shchepetilnikov, I. V. Kukushkin, W. Dietsche, and S. Schmult, *Phys. Rev. B* **83**, 041307(R) (2011).
- [13] A. Usher, R. J. Nicholas, J. J. Harris, and C. T. Foxon, *Phys. Rev. B* **41**, 1129 (1990).
- [14] V. T. Dolgoplov, A. A. Shashkin, A. V. Aristov, D. Schmerek, W. Hansen, J. P. Kotthaus, and M. Holland, *Phys. Rev. Lett.* **79**, 729 (1997).
- [15] I. L. Aleiner and L. I. Glazman, *Phys. Rev. B* **52**, 11296 (1995).
- [16] M. A. Paalanen, D. C. Tsui, and A. C. Gossard, *Phys. Rev. B* **25**, 5566(R) (1982); H. P. Wei, S. Y. Lin, D. C. Tsui, and A. M. M. Pruisken, *ibid.* **45**, 3926 (1992); G. S. Boebinger, Ph.D. thesis, Massachusetts Institute of Technology, 1986; P. T. Coleridge, P. Zawadzki, and A. S. Sachrajda, *Phys. Rev. B* **49**, 10798(R) (1994); L. P. Rokhinson, B. Su, and V. J. Goldman, *Solid State Commun.* **96**, 309 (1992).
- [17] M. M. Fogler and B. I. Shklovskii, *Phys. Rev. B* **52**, 17366 (1995).
- [18] S. Dietrich, S. Vitkalov, D. V. Dmitriev, and A. A. Bykov, *Phys. Rev. B* **85**, 115312 (2012).
- [19] J. Q. Zhang, S. Vitkalov, and A. A. Bykov, *Phys. Rev. B* **80**, 045310 (2009).
- [20] N. C. Mamani, G. M. Gusev, O. E. Raichev, T. E. Lamas, and A. K. Bakarov, *Phys. Rev. B* **80**, 075308 (2009).
- [21] N. Romero, S. McHugh, M. P. Sarachik, S. A. Vitkalov, and A. A. Bykov, *Phys. Rev. B* **78**, 153311 (2008).
- [22] E. I. Rashba, *Sov. Phys. Solid State* **2**, 1109 (1960).
- [23] Yu. A. Bychkov and E. I. Rashba, *JETP Lett.* **39**, 78 (1984).
- [24] J. M. Ziman *Principles of the Theory of Solids* (Cambridge University Press, New York, 1972).
- [25] M. G. Vavilov and I. L. Aleiner, *Phys. Rev. B* **69**, 035303 (2004).
- [26] P. T. Coleridge, *Semicond. Sci. Technol.* **5**, 961 (1990).
- [27] D. R. Leadley, R. Fletcher, R. J. Nicholas, F. Tao, C. T. Foxon, and J. J. Harris, *Phys. Rev. B* **46**, 12439 (1992).
- [28] M. E. Raikh and T. V. Shahbazyan, *Phys. Rev. B* **49**, 5531 (1994).
- [29] O. E. Raichev, *Phys. Rev. B* **78**, 125304 (2008).
- [30] W. Mayer, J. Kanter, J. Shabani, S. Vitkalov, A. K. Bakarov, and A. A. Bykov, *Phys. Rev. B* **93**, 115309 (2016).
- [31] S. A. Vitkalov, H. Zheng, K. M. Mertes, M. P. Sarachik, and T. M. Klapwijk, *Phys. Rev. Lett.* **85**, 2164 (2000); S.A.V. thanks Prof. M. E. Raikh for the indication of the relevance of the observed product of the spin-up and spin-down density of states to a spin inter-subband scattering.
- [32] S. A. Vitkalov, H. Zheng, K. M. Mertes, M. P. Sarachik, and T. M. Klapwijk, *Phys. Rev. B* **63**, 193304 (2001).
- [33] S. A. Vitkalov, *Phys. Rev. B* **64**, 195336 (2001).
- [34] V. F. Gantmakher and Y. B. Levinson, *Carrier Scattering in Metals and Semiconductors* (North-Holland, Amsterdam, 1987).
- [35] I. A. Dmitriev, M. G. Vavilov, I. L. Aleiner, A. D. Mirlin, and D. G. Polyakov, *Phys. Rev. B* **71**, 115316 (2005).
- [36] E. M. Baskin, L. I. Magarill, and M. V. Entin, *Sov. Phys. JETP* **48**, 365 (1978).
- [37] M. M. Fogler, A. Yu. Dobin, V. I. Perel, and B. I. Shklovskii, *Phys. Rev. B* **56**, 6823 (1997).

- [38] D. G. Polyakov, F. Evers, A. D. Mirlin, and P. Wolfle, *Phys. Rev. B* **64**, 205306 (2001).
- [39] J.-q. Zhang, S. Vitkalov, A. A. Bykov, A. K. Kalagin, and A. K. Bakarov, *Phys. Rev. B* **75**, 081305(R) (2007).
- [40] A. T. Hatke, M. A. Zudov, L. N. Pfeiffer, and K. W. West, *Phys. Rev. B* **83**, 081301(R) (2011).
- [41] A. Bogan, A. T. Hatke, S. A. Studenikin, A. Sachrajda, M. A. Zudov, L. N. Pfeiffer, and K. W. West, *Phys. Rev. B* **86**, 235305 (2012).
- [42] R. G. Mani, *Phys. Rev. B* **72**, 075327 (2005).
- [43] C. L. Yang, R. R. Du, L. N. Pfeiffer, and K. W. West, *Phys. Rev. B* **74**, 045315 (2006).
- [44] S. Hikami, A. I. Larkin, and Y. Nagaoka, *Prog. Theor. Phys.* **63**, 707 (1980).
- [45] S. V. Iordanskii, Yu. B. Lyanda-Geller, and G. E. Pikus, *JETP Lett.* **60**, 206 (1994).
- [46] Y. Araki, G. Khalsa, and A. H. MacDonald, *Phys. Rev. B* **90**, 125309 (2014).
- [47] T. Hassenkam, S. Pedersen, K. Baklanov, A. Kristensen, C. B. Sorensen, P. E. Lindelof, F. G. Pikus, and G. E. Pikus, *Phys. Rev. B* **55**, 9298 (1997).
- [48] J. B. Miller, D. M. Zumbuhl, C. M. Marcus, Y. B. Lyanda-Geller, D. Goldhaber-Gordon, K. Campman, and A. C. Gossard, *Phys. Rev. Lett.* **90**, 076807 (2003).
- [49] Z.-F. Jiang, S.-Q. Shen, and F.-C. Zhang, *Phys. Rev. B* **80**, 195301 (2009).
- [50] C. L. Yang, J. Zhang, R. R. Du, J. A. Simmons, and J. L. Reno, *Phys. Rev. Lett.* **89**, 076801 (2002).
- [51] M. G. Vavilov, I. L. Aleiner, and L. I. Glazman, *Phys. Rev. B* **76**, 115331 (2007).
- [52] W. Mayer, S. Vitkalov, and A. A. Bykov, *Phys. Rev. B* **93**, 245436 (2016).